Tectonophysics xxx (2015) xxx–xxx

Contents lists available at ScienceDirect

Tectonophysics

journal homepage: www.elsevier.com/locate/tecto

Rapid deformation rates due to development of diapiric anticline in southwestern Taiwan from geodetic observations

Kuo-En Ching [a,*], Jonathan R. Gourley [b,1], Yuan-Hsi Lee [c,2], Shu-Chin Hsu [d,3], Kwo-Hwa Chen [e,4], Chien-Liang Chen [f,5]

[a] Department of Geomatics, National Cheng Kung University, Taiwan 1 University Rd., Tainan 701, Taiwan
[b] Trinity College, 300 Summit Street, Hartford, CT 06106, USA
[c] Department of Earth and Environmental Sciences, National Chung Cheng University, 168 University Rd., Min-Hsiung, Chia-Yi 621, Taiwan
[d] Department of Geomatics, National Cheng Kung University, 1 University Rd., Tainan 701, Taiwan
[e] Department of Real Estate and Built Environment, National Taipei University, 151 University Rd., San-Shia, Taipei 23741, Taiwan
[f] Central Geological Survey, Ministry of Economic Affairs, No. 2, Ln. 109, Huaxin St., Zhonghe Dist., New Taipei City 235, Taiwan

ARTICLE INFO

Article history:
Received 4 March 2015
Received in revised form 16 June 2015
Accepted 26 July 2015
Available online xxxx

Keywords:
GPS
Precise leveling measurement
Hsiaokangshan fault
Chishan fault
2D kinematic fault model
Mud diapir

ABSTRACT

We adopted 106 campaign-mode GPS observations and 310 precise leveling measurements between 2002 and 2010 to understand the present-day crustal deformation in mudstone area and to estimate the earthquake potential of the Hsiaokangshan (HKSF) and the Chishan faults (CHNF) in southwest Taiwan. Horizontal velocities east of the CHNF are ~66 mm/yr, 270° and gradually decrease westward to ~15 mm/yr, N259°. A horizontal velocity gradient of ~15 mm/yr is shown between the HKSF and CHNF. Subsidence rates west of the HKSF and east of the CHNF are ~5–10 mm/yr, while the uplift is observed between these two faults in the highest elevation with the maximum rate of ~18 mm/yr. The observed deformation patterns are difficult to be fully modeled by 2D kinematic fault model. Field relationships within the vertical shear zones of the mudstone therefore indicate that the deformation pattern may be also controlled by a relic onshore mud diapir that is still experiencing vertical uplift. Consistency between the geological and geodetic vertical velocities, weak rock strength, and no destructive earthquakes over the last 100 years imply that faults (HKSF) within the mudstone area are creeping. However, the CHNF or the associated décollement may still have earthquake potential.

1. Introduction

The stress accumulated due to the high surface shortening rate measured by geodetic surveys due to the friction on reverse fault planes is proposed to be released by earthquakes in the compressive environment [e.g., Kostrov, 1974; Savage and Simpson, 1997]. In this condition, an anticlinal landform grows due to the formation of thrust-related anticline [e.g., Lacombe et al., 1997, 2004]. However, the anticlinal landform is also the apparent topographic feature of the mud diapir because of ascending of the buried sediments due to buoyancy contrast in materials [Kopf, 2002]. The mud diapir, an upward migrating mass of buoyant, clay-rich sediment but not piercing all of its overburden rock, is usually related to regional compressive stresses, too [Hedberg, 1974; Jenyon, 1986; Magara, 1978; Shih, 1967; Sumner and Westbrook, 2001; Kopf, 2002; Franek et al., 2014]. In other words, the upward migration of mud diapir will reduce the estimated seismic hazard. Therefore how to distinguish the mechanisms of the thrust-related anticline and mud diapir in the high shortening region is an important issue to evaluate the earthquake potential.

Southwest Taiwan (the Kaoping region) (inset of Fig. 1a) contains the second largest city in Taiwan, Kaohsiung metropolitan area, at the western Kaoping region with more than 2.7 million people and two national freeways and one high speed railroad pass through this area (Fig. 1a). This region is an excellent experimental field to answer the foresaid question because of the high contraction rate of ~1.0 μstrain/yr and right-lateral shearing inferred from previous sparse GPS horizontal velocities [Bos et al., 2003; Chang et al., 2003; Ching et al., 2007b, 2011b; Hsu et al., 2009], suggesting that there is a potential for a large seismic event. However, the historical earthquake records indicate that no significant earthquakes have occurred within the last century [Cheng and Yeh, 1989]. Therefore does it mean a large earthquake being coming in SW Taiwan in the near future because seldom earthquakes occurred in this area, such that the *M* 8.8 Maule earthquake occurs at a seismic gap in a subduction zone [e.g., Moreno et al., 2010]?

* Corresponding author. Tel.: +886 6 275 7575x63840; fax: +886 6 237 5764.
E-mail addresses: kuenmiao@yahoo.com.tw, jingkuen@mail.ncku.edu.tw (K.-E. Ching), jonathan.gourley@trincoll.edu (J.R. Gourley), seilee@eq.ccu.edu.tw (Y.-H. Lee), monica198574@yahoo.com.tw (S.-C. Hsu), khchen@mail.ntpu.edu.tw (K.-H. Chen), surveydo@moeacgs.gov.tw (C.-L. Chen).
[1] Tel.: +1 860 297 4128.
[2] Tel.: +886 5 272 0411x66212.
[3] Tel.: +886 6 275 7575x63840.
[4] Tel.: +886 2 2674 8189x67421.
[5] Tel.: +886 2 2946 2793.

http://dx.doi.org/10.1016/j.tecto.2015.07.020
0040-1951/

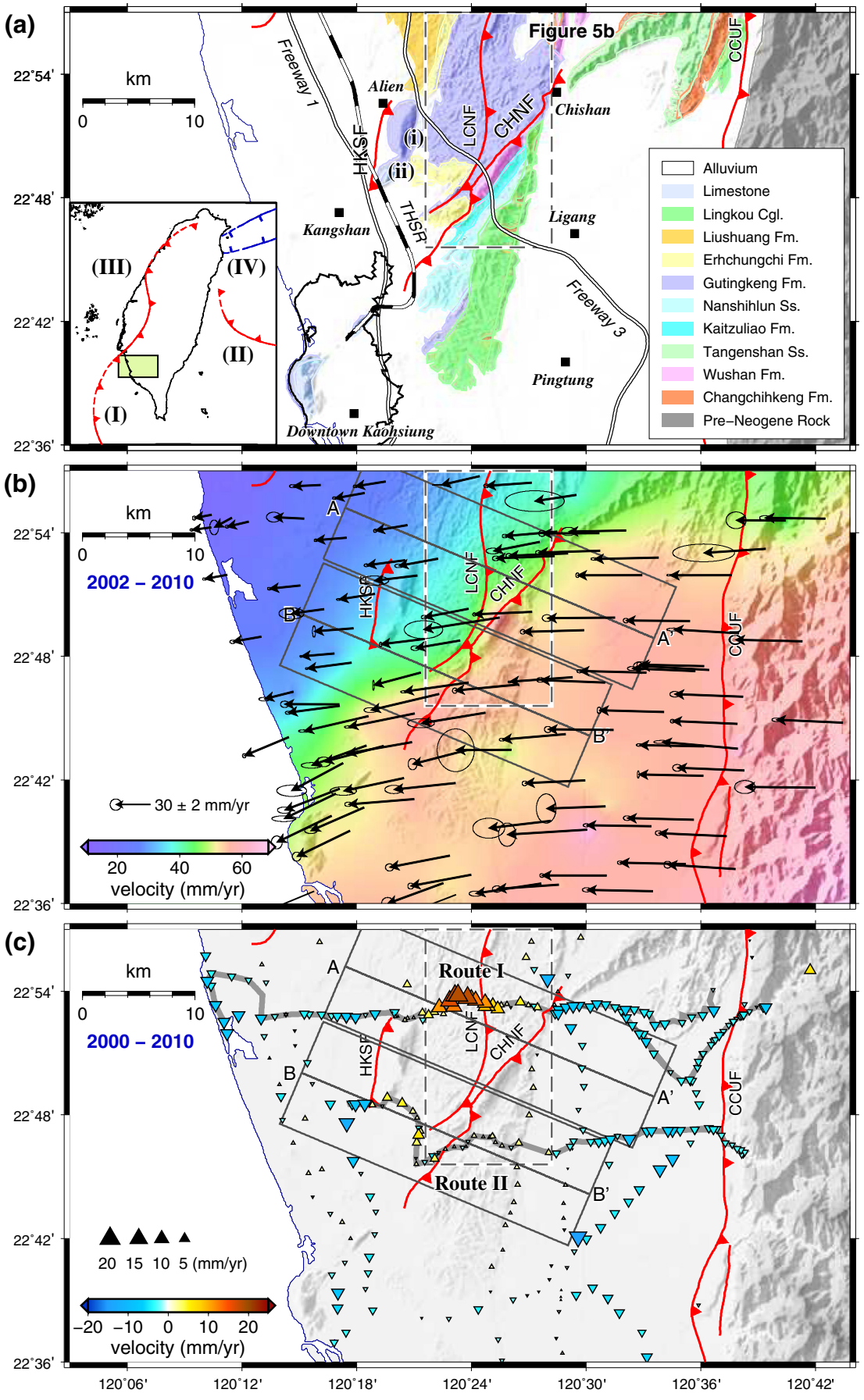

Please cite this article as: Ching, K.-E., et al., Rapid deformation rates due to development of diapiric anticline in southwestern Taiwan from geodetic observations, Tectonophysics (2015), http://dx.doi.org/10.1016/j.tecto.2015.07.020

On the other hand, the inland mud diapirs with reefal limestones have been also observed in southwest Taiwan [Huang et al., 2004; Sun and Liu, 1993]. Is this high strain being accommodated by the development of mud diapir with low potential for major seismicity?

This study combines 106 campaign-mode GPS station data and 310 leveling measurements collected by the Central Geological Survey and the Ministry of Interior, Taiwan between 2000 and 2010 to characterize the deformation pattern within the region of high contraction in southwest Taiwan. A classical 2D fault model is adopted to examine the mechanism of high strain rates and to estimate the potential for generating large earthquakes in the future. Field relationships of faults within the deformation zone are also considered to reconcile a discrepancy between the observed surface deformation and the 2D modeling results. We conclude that the deformation in southwest Taiwan could be a hybrid between relic mud diapirism (vertical tectonics) and fold-and-thrust shortening (horizontal tectonics).

2. Tectonic settings

The Taiwan mountain belt is an ongoing arc–continent collision zone, resulting from the late Cenozoic oblique convergence between the Luzon volcanic arc of the Philippine Sea Plate and the passive continental margin of the Eurasian plate [Angelier et al., 1986; Barrier and Angelier, 1986; Ho, 1986; Huang et al., 1997; Suppe, 1984; Teng, 1990; Byrne et al., 2011] (inset of Fig. 1a). The Philippine Sea Plate moves northwestward relative to the continental margin (the Penghu Islands) with a rate of about 82 mm/yr [Yu et al., 1997]. According to analyses of the GPS velocities, strain rates, and block modeling results, our study area is located within the "deforming domain" proposed by Ching et al. (2007b, 2011b). The strong internal E–W shortening of 0.22–0.92 μstrain/yr, with obvious clockwise rotation of 14.5°–27.1°/Myr, and right-lateral shearing are represented in this area between the deformation front and the Chishan fault (i.e., most parts of the Western Foothills) [Bos et al., 2003; Chang et al., 2003; Ching et al., 2007b, 2011b; Hsu et al., 2009] (the area west of the Chishan fault in Fig. 1a). Based on the principal strain rate orientations and the presence of NNE-striking faults, the multiple reverse faults with a minor right-lateral slip component have been proposed to be active within this domain [Ching et al., 2011b].

2.1. Geology

Our study area (Kaoping region) is located in the regional transition zone from subduction to collision, and consists of Miocene shallow marine deposits and Plio-Pleistocene foreland basin rocks [Lin and Watts, 2002; Teng, 1987]. In this study we mainly focus on the north-central area comprised by the Wushan Formation (Ws) and the Gutingkeng Formation (Gtk) (Fig. 1a).

The Ws (Fig. 1a) is exposed as a prominent topographic ridge. The age of this formation is close to the Tangenshan sand stone in the early Miocene. The maximum thickness of the Ws is 1360 m. Its major composition is gray to ochroid fine sand stone and dark gray sandy shale, and sometimes interlaces thin sand stone intercalated with shale [Chou, 1971].

The Plio-Pleistocene Gtk dominates the study area and forms a well exposed badland topography throughout the region. The Gtk consists of gray sandy siltstone and sandy mudstone intercalated with lenticular greywacke and subgraywacke with abundant Mollusca [Chou, 1971] (Fig. 1a). The thickness of this formation is 540–1000 m. The Upper Gtk is erosion resistant and appears as 4–5 m prominent layer. The bottom of Gtk formation is conformable with the older Ws.

Two anticlinal landforms in southwest Taiwan are noteworthy structural features: the Takangshan hill and the Hsiaokangshan hill (Fig. 1a), which were proposed to be topographic features related to mud diapirs because of analogous offshore mud diapirs with reefal limestone caps [Sun and Liu, 1993; Huang et al., 2004]. However, due to the asymmetry of the anticlinal landform, the mud diapir hypothesis was rejected by Lacombe et al. (1997, 2004) and west vergent thrust-related anticlines were proposed as an alternative origin of these anticlinal mudstones.

2.2. Active faults

Concurrent with the development of the active anticlinal landforms, three major faults, the Chishan fault (CHNF), Lungchuan fault (LCNF), and Hsiaokangshan fault (HKSF) from east to west (Fig. 1a), are examined in this study. Based on the field investigations and analyses of geophysical data, the CHNF and the HKSF were classified as first class and second class active faults, respectively, by the Central Geological Survey (CGS) in 2010.

The HKSF forms the western boundary of the Takangshan and Hsiaokangshan hills [Sun, 1964] (Fig. 1a). The length of the NNE-striking HKSF is ~8 km and DEM analysis indicates an obvious fault scarp [Hsu and Chang, 1979; Sun, 1964]. However, the exact location of the HKSF is still unclear because the scarp has been eroded and therefore the fault surface is poorly exposed in the field. Previous seismic studies indicate that the HKSF is an east-dipping thrust fault [Hsu and Chang, 1979; Sun, 1964]. In addition, based on carbon-14 dating from 4 wells near the HKSF, and the assumption of an ~45°, east-dipping fault the net long-term slip rate of the HKSF is estimated to be 5.7 ± 1.4 mm/yr [*CGS Report*, 2009].

The LCNF (Fig. 1a) has been proposed as a reverse fault with low dip angle with the thickness of fault gouge observed from the outcrop as ~20–30 m [Huang et al., 2004]. The strike of the northern LCNF is ~N–S orientation while the strike of the southern LCNF is about N30°–40°E (Fig. 1a). In addition, the fault dip angle also becomes steeper to the north. The LCNF might be a thrust along the hinge of the anticline. From the seismic reflection profile, the anticline has been inferred as the fault propagation fold [Cheng, 2000].

The NE-trending CHNF, composed of a major fault and several branching segments, separates the Gtk mudstone to the west (footwall) and the Ws to the east (hanging wall) (Fig. 1a). Data on the sense of shear of the CHNF has proven to be ambiguous. Slickenside analysis result along the fault trace suggests the CHNF to be a reverse fault with a left-lateral component [Hsieh, 1970; Hsu and Chang, 1979; Tsan and Keng, 1968; Chen, 2005]. However, the analysis of GPS data across the CHNF indicates that the fault is a reverse fault with a right-lateral component [Ching et al., 2007b, 2011b; Hu et al., 2007; Lacombe et al., 2001]. Gourley et al. (2012) mapped vertical shear zones within the CHNF that contained normal sense of shear indicators that suggest the Gtk has moved vertically (up) relative to the Ws.

3. Geodetic data acquisition

3.1. Campaign-mode GPS observations

We used the GPS observations from 106 GPS stations installed by the CGS in our study area in SW Taiwan from 2002 to 2010 (Fig. 1b). GPS

Fig. 1. (a) Geological background. Blue triangles are campaign-mode GPS stations. Thick black line shows the downtown of Kaohsiung city. THSR is Taiwan high speed railroad. Background is the geological formations in our study area. Red lines denote the locations of the active faults. HKSF: the Hsiaokangshan fault, LCNF: the Lungchuan fault, CHNF: the Chishan fault, CCUF: the Chaochou fault. (i) denotes the Takangshan hill and (ii) denotes the Hsiaokangshan hills. Dashed gray rectangle indicates the location of Fig. 5b. The inset shows the tectonic frame of Taiwan. Green square denotes the study area. (I) Manila trench; (II) Ryukyu trench; (III) deformation front; (IV) Okinawa trough. (b) Horizontal velocities relative to the station S01R from 2002 to 2010. Arrows denote the vectors derived by campaign-mode GPS observations. Ellipses at the tips of vectors are the 95% confidence interval. Color scale is the magnitude of the velocity. Gray rectangles show the locations of velocity profiles AA′ and BB′. Dashed gray rectangle indicates the location of Fig. 5b. (c) Vertical velocity field during 2000–2010. Warm-colored triangles denote uplift; cool-colored inverse triangles represent subsidence. Gray lines (Route I and Route II) are the leveling routes installed by the Central Geological Survey, Taiwan. Color scale is the magnitude of the velocity. (For interpretation of the references to color in this figure legend, the reader is referred to the web version of this article.)

Please cite this article as: Ching, K.-E., et al., Rapid deformation rates due to development of diapiric anticline in southwestern Taiwan from geodetic observations, Tectonophysics (2015), http://dx.doi.org/10.1016/j.tecto.2015.07.020

surveys were generally carried out annually. A station is usually occupied by more than two sessions per year. Each session is 6–14 h and all available satellites are tracked and rising higher than a 15° elevation angle. The sampling interval for data logging is 15 s. For about 43% of GPS sites, GPS campaigns spanned more than 6 years. For about 37% of GPS stations, GPS campaigns spanned between 2.5 and 6.0 years. The remaining campaigns spanned about 1.0–2.5 years.

The campaign-surveyed GPS data were processed session by session with Bernese software v.5.0 [Dach et al., 2007] to obtain the precise station coordinates. The precise ephemerides provided by International GNSS Service (IGS) were employed and fixed during the processing. Four global IGS fiducial stations surrounding Taiwan (TSKB, GUAM, PERT and IISC) on the international terrestrial reference frame (ITRF2005) [Altamimi et al., 2007] were used to determine the daily position solutions of 106 GPS stations in our study area. The horizontal uncertainties of station coordinates are estimated to be 2–5 mm. However, the vertical uncertainties are much larger, approximately 10–20 mm. Because of the relatively large uncertainty in the vertical component in our results, we only adopt the horizontal GPS observations in this paper.

3.2. Precise leveling data

The leveling measurements used here are collected from two ~E–W-trending precise leveling routes installed by the CGS with the benchmark-spacing of ~1 km (Fig. 1c). The leveling data were mostly collected at night by Zeiss DiNi-12 digital leveling instruments with invar rods supported by corresponding struts. The precise leveling surveys have been generally carried out annually. The first CGS leveling transect is 91 km in length and crosses the northern side of Takangshan hill. The second transect is 50 km in length and traverses the southern region of Hsiaokangshan hill. These two leveling lines were repeatedly surveyed six times from 2004 to 2010.

Four stringent specifications were applied to the leveling field work in order to reduce or eliminate measurement errors [Chen et al., 2011]. First, the maximum permissible difference in sight lengths between forward and backward sights is 0.5 m per set-up, and the cumulative difference is limited to 1.5 m per section. Second, the maximum length of sight is restricted to 30 m for greatly reducing the influence of atmospheric refraction. The minimum and maximum sight ground clearances are 0.3 m and 2.7 m, respectively. Third, the maximum standard deviation of each leveling reading in a set-up is ± 0.2 mm. Finally, the maximum difference of the two height differences from the double readings at a set-up is limited to 0.4 mm [Chen et al., 2011]. Besides, the maximum misclosure between forward and backward runs in a section is limited to ± 2.0 mm $\sqrt{k}$ (k being the section distance in km). The systematic errors of various kinds were calculated and removed from the measurements, including the invar rod correction from calibration against standard, the invar rod correction for thermal expansion, the curvature correction, and the collimation error [Chen et al., 2011].

4. Surface velocity field

4.1. Horizontal velocity field

In order to characterize the surface deformation of SW Taiwan, we estimate the secular horizontal velocities of GPS stations based on the coordinate time series in a time span of 9 years between 2002 and 2010. Eq. (1) is then used to fit the coordinate time series of nth station and ith coordinate component.

$$x_n^i(t) = a_n^i + b_n^i t + v_n^i \quad (1)$$

Here, $x_n^i(t)$ is the observed displacement of each station at a specific epoch, t, in units of year. a_n^i is the intercept; b_n^i is the linear velocity of the station; and v_n^i is the residual. Next, the horizontal velocities are estimated by least squares in east and north components.

The standard deviation of horizontal velocities was estimated by an empirical function shown in Ching et al. (2011b). We scaled the formal uncertainties ($\boldsymbol{\sigma_{ls}}$) obtained from least squares estimation of velocities by amount $\boldsymbol{k} = (\boldsymbol{mis}/2)^2$. Here $\boldsymbol{k}$ is the effect of daily coordinate variation presented in the coordinate time series, where $\boldsymbol{mis}$ is the residual of calculations and observations for the time series on east and north component, respectively. Then the uncertainty $\boldsymbol{\sigma}$ of velocity for each component is re-estimated by $\boldsymbol{\sigma} = (\boldsymbol{\sigma_{ls}}^2 \times \boldsymbol{k})^{1/2}$.

GPS horizontal velocities are relative to the station S01R at the Penghu Island in the Chinese continental margin (Fig. 1b and Table S1). The horizontal velocities east of the Chishan fault are ~66 mm/yr, N270°. Velocities gradually decrease westward to ~15 mm/yr, N259°. The azimuths of velocities present an apparent counterclockwise rotation from EW to WSW. This rotation has been interpreted as southwestward lateral extrusion within the collision of Taiwan [Ching et al., 2007b; Gourley, 2006; Byrne et al., 2011]. In addition, most azimuths of velocities in the northern area are almost westward. However, the azimuths in the southern area rotate from nearly W (~270°) to WSW (~255°). A notable horizontal velocity gradient is detected between the CHNF and HKSF. A shortening rate of ~15 mm/yr exists from ~50 mm/yr east of the CHNF to ~35 mm/yr west of the HKSF (Fig. 1b).

4.2. Vertical velocity field

The vertical velocities are evaluated by repeated leveling measurements from two CGS precise leveling lines according to the coordinate time series in a time span of 7 years from 2004 to 2010. Eq. (1) is also used to fit the coordinate time series of nth station and ith coordinate component. The reference stations of these two independent precise leveling lines are the westernmost benchmarks of their leveling routes. Due to the sparse distribution of the CGS benchmarks in our study area, the vertical velocity field between 2000 and 2008 published by Ching et al. (2011a) is also adopted to obtain more abundant information of surface vertical deformation. These vertical velocities derived from the leveling data are placed in a reference frame of the Chinese continental margin, station S01R, using 199 continuous GPS observations at nearby sites [Ching et al., 2011a].

To compare these two vertical velocity fields, we have to adjust the CGS leveling vertical velocities into the same reference frame as the published velocities by Ching et al. (2011a). To do this, we compare the differences of vertical velocities between these two datasets at the same observation sites. The difference of vertical velocities is the difference of their vertical velocity reference frames. Twenty benchmarks are chosen for the northern CGS leveling route and the discrepancy of ~−3.9 mm/yr in vertical velocity is estimated. One benchmark is selected for the southern route and the discrepancy of ~−3.6 mm/yr is inferred. Then we remove these discrepancies from two CGS leveling vertical velocity fields and the reference station for the hybrid vertical velocity field is S01R station (Fig. 1c, Tables S2 and S3).

For the vertical velocity field in SW Taiwan, we notice that there is a high correlation between the spatial variation of vertical velocities and the terrain elevation (Fig. 1c). The uplift is mainly represented in the hill area with the maximum uplift rate of ~18 mm/yr located between the HKSF and the CHNF. The subsidence with a rate less than 15 mm/yr is predominately shown in plain domain (Fig. 1c). In the northern study area, the vertical velocities west of the HKSF are subsidence. On the contrary, the velocities gradually increase eastward up to ~18 mm/yr between the HKSF and the CHNF. East of the CHNF, the vertical velocity

Fig. 2. (a) Sketch map of 2-D fault model. (b) Modeling results across the AA′ profile. (c) Modeling results across the BB′ profile. The uppermost panel shows the vertical velocities. The central two panels are horizontal velocities. The lowest panel represents fault geometries and slip rates on the faults. Light circles with error bars are observations while dark circles are model predictions. Dashed lines denote the locations of the major faults extended to the surface.

Please cite this article as: Ching, K.-E., et al., Rapid deformation rates due to development of diapiric anticline in southwestern Taiwan from geodetic observations, Tectonophysics (2015), http://dx.doi.org/10.1016/j.tecto.2015.07.020

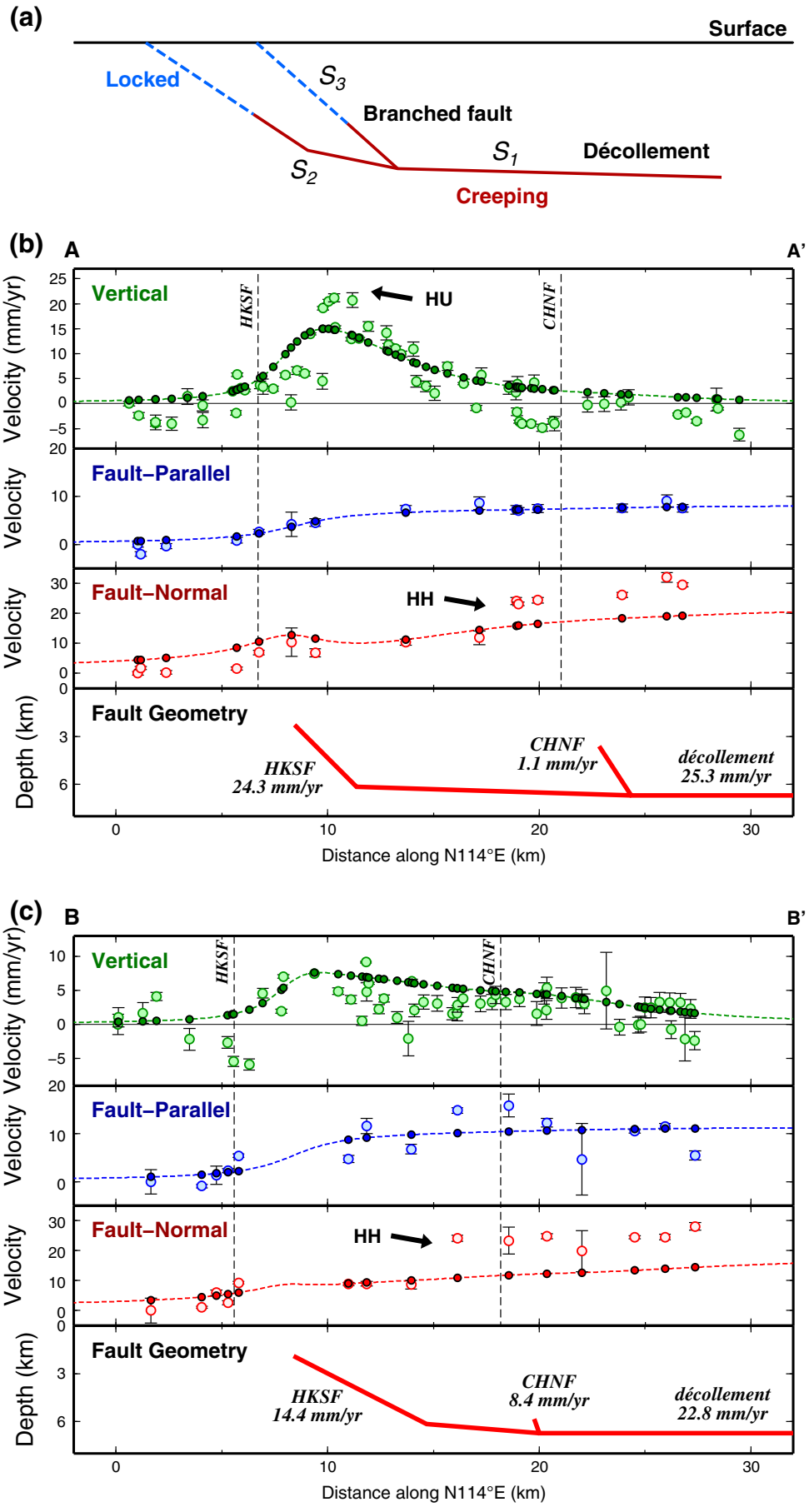

Please cite this article as: Ching, K.-E., et al., Rapid deformation rates due to development of diapiric anticline in southwestern Taiwan from geodetic observations, Tectonophysics (2015), http://dx.doi.org/10.1016/j.tecto.2015.07.020

Table 1
Fault parameters of profiles AA′ and BB′.

Fault name	Profile AA′					
	Dip angle (°)	Depth (km)	Locking depth (km)	Location (km)	Slip rate (mm/yr)	Rake (°)
HKSF	52.9 ± 4.1	6.2 ± 0.1	2.3 ± 0.2	6.7 ± 0.2	24.3 ± 1.6	107.9 ± 2.1
CHNF	63.8 ± 8.5	6.7 ± 0.1	3.6 ± 1.8	21.0 ± 1.1	1.1 ± 0.9	133.2 ± 8.2
Décollement	~0	–	–	–	25.3 ± 1.5	109.2 ± 1.9
	Profile BB′					
HKSF	34.0 ± 2.5	6.1 ± 0.1	1.9 ± 0.2	5.6 ± 0.3	14.4 ± 0.8	133.6 ± 3.7
CHNF	74.9 ± 6.4	6.7 ± 0.1	5.8 ± 0.5	18.2 ± 0.8	8.4 ± 0.3	96.7 ± 3.7
Décollement	~0	–	–	–	22.8 ± 0.8	120.9 ± 2.3

HKSF: the Hsiaokangshan fault; CHNF: the Chishan fault.

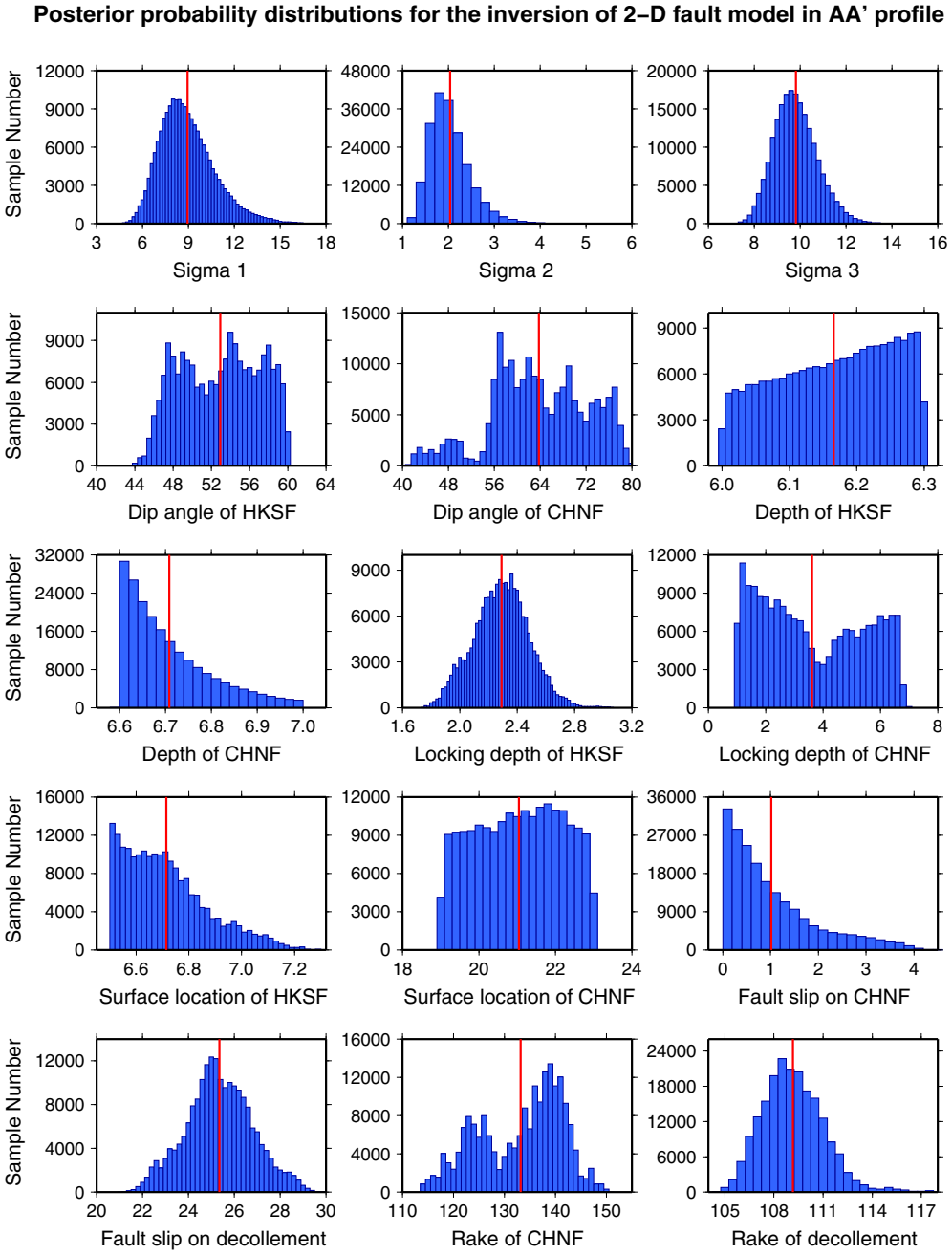

Fig. 3. Posterior probability distributions for the inversion of 2-D fault model in AA′ profile. Red vertical lines indicate the mean values. Sigma 1, sigma 2 and sigma 3 are the covariance weights of fault-normal horizontal component data, fault-parallel horizontal component data and vertical data, respectively. (For interpretation of the references to color in this figure legend, the reader is referred to the web version of this article.)

Please cite this article as: Ching, K.-E., et al., Rapid deformation rates due to development of diapiric anticline in southwestern Taiwan from geodetic observations, Tectonophysics (2015), http://dx.doi.org/10.1016/j.tecto.2015.07.020

is then subsided again (Fig. 1c). The vertical velocities in the central study area show subsidence west of the HKSF. The velocities increase eastward to ~6 mm/yr between the HKSF and the CHNF. East of the CHNF, the velocities decrease to almost zero. Further to the east, the vertical velocities show subsidence again in the Pingtung plain. The land subsidence west of the HKSF results from the artificial groundwater withdrawal by the factories. However, the reason of subsidence in the Pingtung plain remains unclear.

5. 2-D fault models

In order to analyze the kinematics of major faults in southwestern Taiwan, the horizontal and vertical velocities from two velocity profiles are inverted for the fault slip rates and fault geometries using a 2-D fault model. The horizontal velocities here are decomposed into the fault-parallel and fault-perpendicular components. Two velocity profiles are chosen across the HKSF, the LCNF, and the CHNF (Fig. 1b and c). Because the slip rate of the LCNF is insignificant and location of this fault is unreasonable after several tests, the LCNF is not included in this model.

For the 2-D fault model, we first assume that the fault geometry consists of a décollement and several branched faults after Johnson et al. (2005) (Fig. 2a). The décollement is assumed to be creeping, that is, no strain accumulation on the décollement. The slip rate on the décollement (S_1) is the summation of the slip rates on all the branched faults (S_2 and S_3) (Fig. 2a). Due to the effect of friction on the fault, the shallow segment of the branched fault might be locked and accumulate

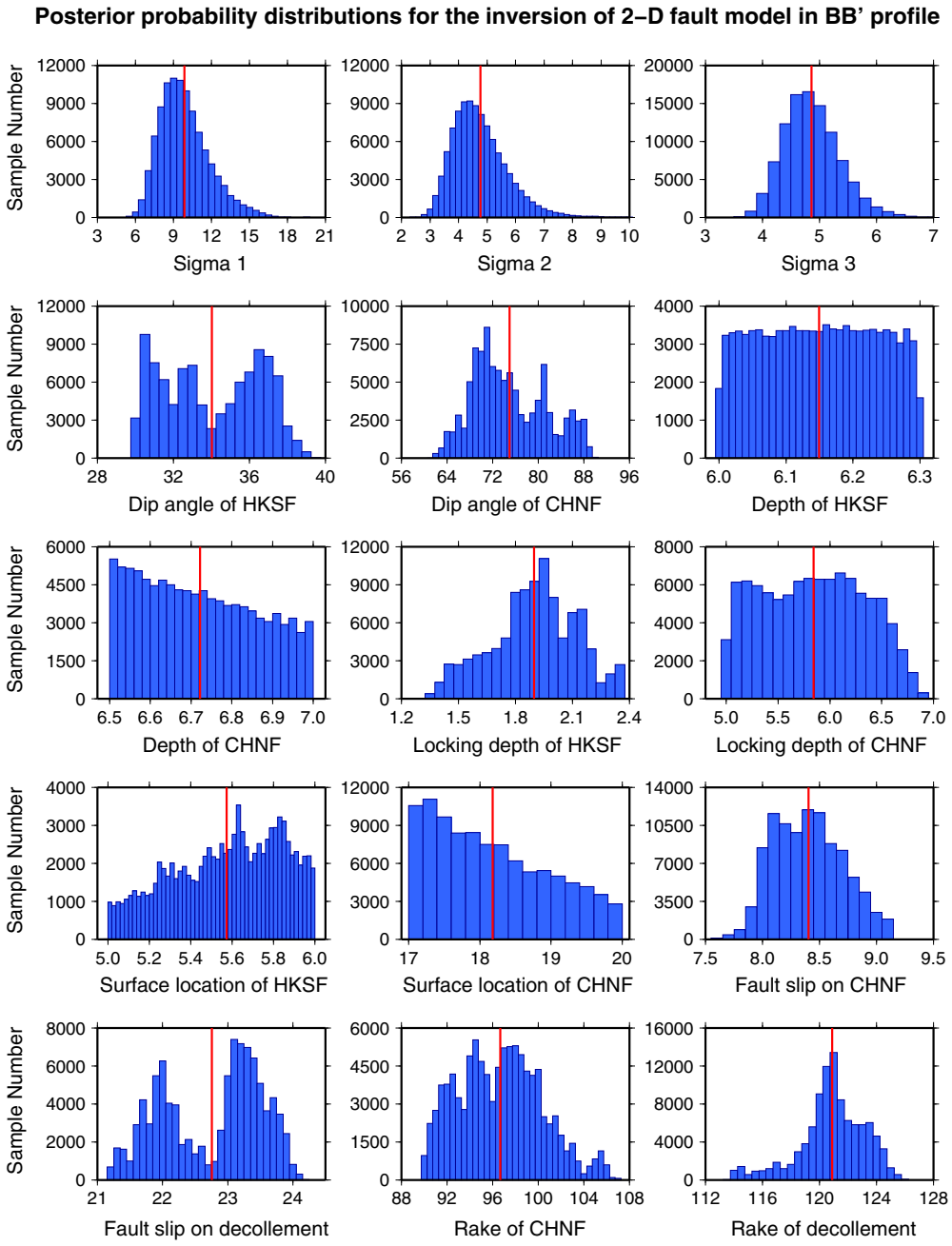

Fig. 4. Posterior probability distributions for the inversion of 2-D fault model in BB′ profile. Red vertical lines indicate the mean values. Sigma 1, sigma 2 and sigma 3 are the covariance weights of fault-normal horizontal component data, fault-parallel horizontal component data and vertical data, respectively. (For interpretation of the references to color in this figure legend, the reader is referred to the web version of this article.)

Please cite this article as: Ching, K.-E., et al., Rapid deformation rates due to development of diapiric anticline in southwestern Taiwan from geodetic observations, Tectonophysics (2015), http://dx.doi.org/10.1016/j.tecto.2015.07.020

the energy during the interseismic period. This model simply assumes that the slip rate on the segment shallower than the locking depth is zero. The relationship between the fault geometry and the fault slip rate is illustrated by the Green's function from Okada (1985). The fault parameters used in this model are fault dip angle, depth, locking depth, locations of faults at surface, slip rates and rake angles (Table 1). We search the optimized fault parameters using the Monte Carlo-Metropolis inversion. The details of the Monte Carlo inversion algorithm are described in Fukuda and Johnson (2008). To sample the a posteriori distribution, we initiate Markov Chain random walk through the model space directed by the so-called Metropolis step. The RMS value is defined as follows

$$\mathrm{RMS} = \sqrt{\frac{(\mathbf{As}-\mathbf{data})^2}{dof}}. \quad (2)$$

Here, **A** is the Green's function from Okada (1985); **s** is the slip rates on faults; **data** is the observed velocities; and *dof* is degree of freedom.

In this study, the a priori parameters and the searching boundaries of the fault geometries are based on the geological profiles across the Takangshan hill [Lacombe et al., 1997, 1999; Mouthereau et al., 2002]. The locations of the HKSF and the CHNF are proposed by the CGS in 2010. To discard the surface deformation contributed by the westward extended décollement from the HKSF, all the modeled data are relative to the westernmost station in the selected profiles.

5.1. AA′ profile

In the AA′ velocity profile, no remarkable velocity discontinuity is represented across the HKSF (Fig. 2b). However, a notable shortening of ~10 mm/yr with dextral strike-slip component of ~8 mm/yr between the HKSF and the CHNF is shown in this profile. Besides, a noteworthy shortening of ~12 mm/yr is represented across the northern segment of the CHNF (HH in Fig. 2b). Nevertheless, the maximum vertical velocity of ~20 mm/yr appears at the location of ~8 km west of the position of the significant shortening (HU in Fig. 2b). Following the uplift around HU in Fig. 2b, minor localized extension is observed on the hanging wall of the HKSF (Fig. 2b). However, the spatial coverage of GPS stations here is too sparse to strongly prove the localized deformation.

According to the best-fit model, the RMS is 2.2 mm/yr and the surface deformation is significant, with both the décollement (25.3 mm/yr) and the HKSF (24.3 mm/yr) contributing to the total slip (Fig. 2b and Table 1). The posterior probability distributions for the inversion are shown in Fig. 3. Here we notice that it is hard to model the high uplift rate at the location of ~10 km (HU in Fig. 2b) and ~12 mm/yr shortening rate at location of ~18 km (HH in Fig. 2b) simultaneously. If these velocity changes are caused by the fault slip, their positions should be comparable.

5.2. BB′ profile

In the BB′ profile, no notable velocity gradient is observed across the HKSF (Fig. 2c). However, the relatively high uplift rates of ~5 mm/yr are shown at the location of ~10 km (Fig. 2c). An obvious shortening with the rate of ~15 mm/yr is observed between the HKSF and CHNF (HH in Fig. 2c); while a right-lateral strike-slip component with the rate of ~16 mm/yr is also shown in this profile.

The RMS of the optimal model in BB′ profile is 1.3 mm/yr and the posterior probability distributions for the inversion are shown in Fig. 4. The major slip rate shows that the surface deformation is primarily caused by the décollement (22.8 mm/yr), HKSF (14.4 mm/yr), and CHNF (8.4 mm/yr) (Fig. 2c and Table 1). However, we also notice that an ~15 mm/yr shortening rate at location of ~15 km (HH in Fig. 2c) is hard to be modeled (Fig. 2c).

6. Mechanism of mud rising across the Gutingkeng Formation (Gtk)

Dislocation models have been adopted for successfully estimating the slip rates on active faults in central Taiwan [e.g., Hsu et al., 2003; Tsai et al., 2012]. However, in terms of our modeling results (Fig. 2),

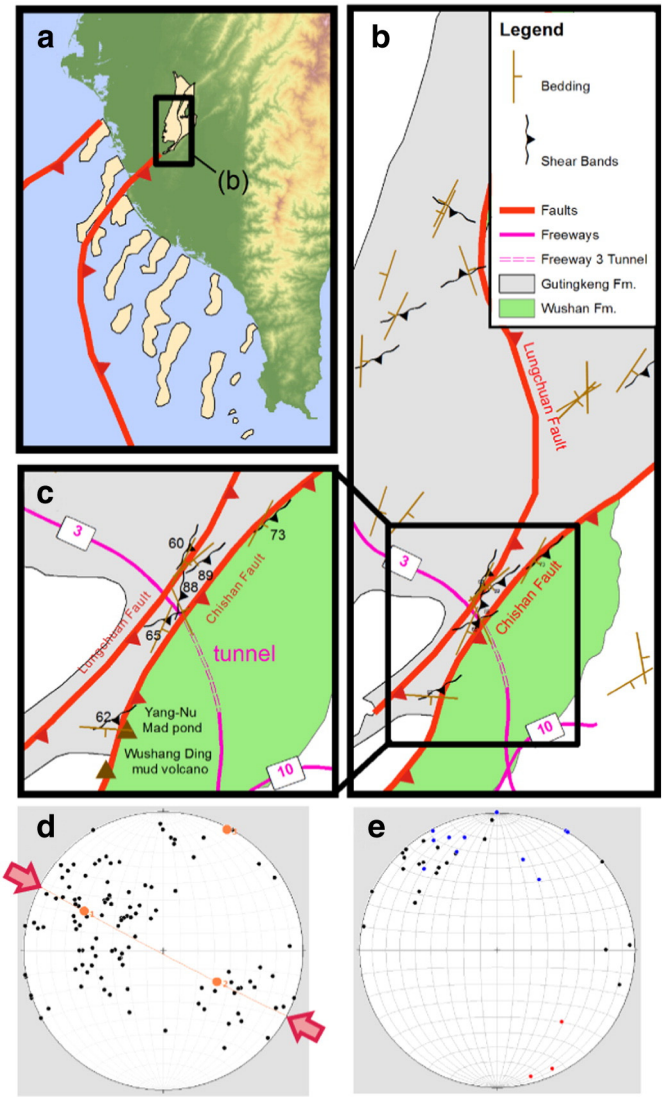

Fig. 5. (a) Tan regions depict southern Taiwan distribution of offshore mud diapirs (modified from Chuang (2006)) and onshore Gutingkeng mudstone (Gtk) aerial extent. The major faults drawn represent accretionary wedge thrusts. The easternmost of these thrusts continues on shore and is manifested/projected as the Chishan fault. The map pattern of the Gtk is similar in shape and size to the offshore mud diapirs. The smaller inset box within (a) shows the extent of map (b). Panels (b) and (c) are geologic and structural maps of the southern Gutingkeng Formation. Panel (b) covers the extent of structural mapping and panel (c) is a zoomed in region along the Chishan fault. Exposures are excellent in this region as the mudstones have developed into a badland topography. Bedding (brown strike and dip symbols) is mapped across the Gtk and is folded into anticlinorium as summarized in (d), a southern hemisphere stereo projection of all poles to bedding (n = 113; trend and plunge of fold axis = 028/02). The direction of shortening is 296° which is typical of many Taiwan folds and is parallel to the plate convergent vector of the Taiwan collision. (e) The distribution of shear bands in three discrete regions within the Gtk. In all cases the shear bands are not parallel to bedding and are vertical or very steeply dipping; black poles = Eastern region, n = 22; blue poles = western region, n = 11; and red poles = northern region, n = 3. In all locations where the sense of shear of the shear bands was observed the interior of the Gtk was moving up relative to peripheral blocks. (For interpretation of the references to color in this figure legend, the reader is referred to the web version of this article.)

Please cite this article as: Ching, K.-E., et al., Rapid deformation rates due to development of diapiric anticline in southwestern Taiwan from geodetic observations, Tectonophysics (2015), http://dx.doi.org/10.1016/j.tecto.2015.07.020

the deformation patterns are difficult to be modeled well in both profiles. Therefore the slip alone along the HKSF and CHNF is not the only mechanism that can explain the vertical component of the Gtk mudstones. A geologic investigation of the Gtk has revealed a second possible mechanism that may contribute to the uplift of the region.

Vertical shear zones were mapped throughout the Gtk and are not limited to major fault zone regions (Fig. 5). These shear zones cross-cut bedding in all observed cases and range in dip from 58° to 90°. Thickness of the shear bands range from several centimeters to 10s of meters. Exposure of the Gtk is very good due to the badlands topography created by the eroding muds. The shear bands are frequently observed in the proximity of the CHNF but are found in outcrops in the western and northern areas of the Gtk as well (Fig. 5). Initial mapping focused on the region near the CHNF to determine the sense of shear of the fault zone [Sobolewski and Gourley, 2008]. Despite the CHNF being mapped as a top to the west reverse fault (Ws over the Gtk), all sense of shear indicators indicated a normal displacement along steeply dipping or vertical shear bands (Fig. 5). This sense of shear indicates that the Gtk is rising (at least in part) along these bands relative to the surrounding geology. Unpublished rock cores have been taken along the CHNF in the hanging wall (Ws) and about few meters away from the fault trace. The depth of the cores is over ten meters. However, under the assumption that the dip angle of the CHNF is 70°, they never intersected the anticipated CHNF, further suggesting that boundary between the Gtk and Ws is a steep, if not vertical structure. This inference is consistent with the high dip angle (>60°) at the lower segment of the CHNF inferred from our model (Table 1).

Flexural slip or flexural flow [Donath and Parker, 1964; Ramsay, 1974; Tanner, 1989] is another possible mechanism to produce higher than modeled uplift rates due to the interbedding of sandy siltstone and sandy mudstone in this region. However, in the field no examples of deformations parallel to bedding planes were found. On the contrary, we noticed that the "interior-up" sense of shear zones within the Gtk is consistent with the higher uplift rates (5–15 mm/yr) in the Gtk from leveling measurements than the surrounding geology (Figs. 1c and 5). It is possible that the vertical shear bands throughout the Gtk are accommodating this uplift. Therefore we interpret the collective field evidence to suggest that the CHNF is a near vertical structure that is accommodating uplift of the Gtk, similar to mechanism by which subaqueous mud diapirs grow [e.g., Hsieh, 1972; Pan, 1968; Shih, 1967]. A chain of mud diapirs is located off the southeastern coast of Taiwan [e.g., Huang, 1995; Chiu et al., 2006; Chuang, 2006] and the Gtk may be the onshore extension of this chain. We interpret that this relic mud diapir is accounting for the underestimation of uplift (Fig. 6).

7. High earthquake potential in SW Taiwan?

A high velocity gradient of ~15 mm/yr exists between the HKSF and the CHNF (Fig. 1b), which corresponds to the high contraction rates of ~0.5–1.5 μstrain/yr derived from previous GPS observations [e.g., Yu and Chen, 1994; Bos et al., 2003; Chang et al., 2003; Ching et al., 2007b]. Based on the 3D block modeling results [Ching et al., 2011b], this velocity gradient indicates a very high slip deficits in southwest Taiwan. That is, an earthquake recurrence interval of less than two hundred years is reasonable in this region of Taiwan. Although the historical earthquake record remains relatively young, the record does lack moderate-to-large scaled earthquakes since 1800 with this region (data source from the Central Weather Bureau). On the other hand, about 2700 $M_L > 2$ earthquakes are detected and only 5 $M_L > 5$ events with their depths > 15 km are found in our study area since 1900 (Fig. 7). However, even these five $M_L > 5$ events are not correlated with the active faults in southwestern Taiwan (Fig. 7). In other words, the high strain rates at the mudstone region of the Gtk may not directly imply the accumulation of the seismic moment.

First, the rock strength of mudstone is weak. Therefore it is difficult to generate large earthquakes within the mudstone area because it is hard to accumulate strain on the fault here during the interseismic period. Second, the short-term uplift rates inferred in our study are very close to the longer-term uplift rates that are observed near the HKSF with the vertical velocities of ~5 mm/yr [Ching et al., 2011a] (Figs. 1c and 7). Hence the high strain rates and the absence of moderate-to-large scaled earthquakes in southwest Taiwan imply that the active faults, such as the HKSF, in the mudstone area may act as creeping faults. However, it is important to keep in mind that creeping faults throughout the world have the potential to generate large earthquake, such as the Parkfield segment of the San Andreas fault in California [Harris and Segall, 1987; Murray et al., 2001] and the Chihshang fault in eastern Taiwan [Ching et al., 2007a]. If we consider that (1) the hanging wall of the CHNF is comprised of sandstone, (2) the locking depth of CHNF is ~6 km in BB′ profile, and (3) deduced historical earthquakes did occur roughly around our study area in 1781–1787 (data source from the Central Weather Bureau), faults in this region could still be capable of producing disastrous earthquakes.

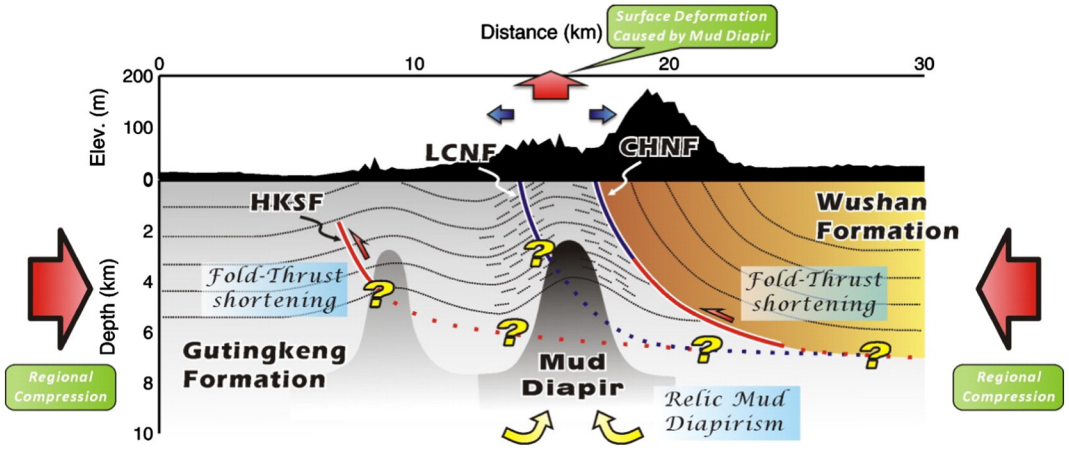

Fig. 6. 2D tectonic kinematic model for SW Taiwan. Red lines are the creeping segments of active faults derived from our modeling result, including the HKSF (the Hsiaokangshan fault) and the CHNF (the Chishan fault). The shallow parts of the CHNF and the LCNF (the Lungchuan fault) shown by blue lines are locked based on our modeling result. Because the simplified dislocation model cannot predict the surface deformation rates well, we propose the mud diapirism as an additional source besides the plate convergence in SW Taiwan. However, the cross-cutting relationship between the mud diapirs and active faults and the presence of décollement remain unclear in this study area. (For interpretation of the references to color in this figure legend, the reader is referred to the web version of this article.)

Please cite this article as: Ching, K.-E., et al., Rapid deformation rates due to development of diapiric anticline in southwestern Taiwan from geodetic observations, Tectonophysics (2015), http://dx.doi.org/10.1016/j.tecto.2015.07.020

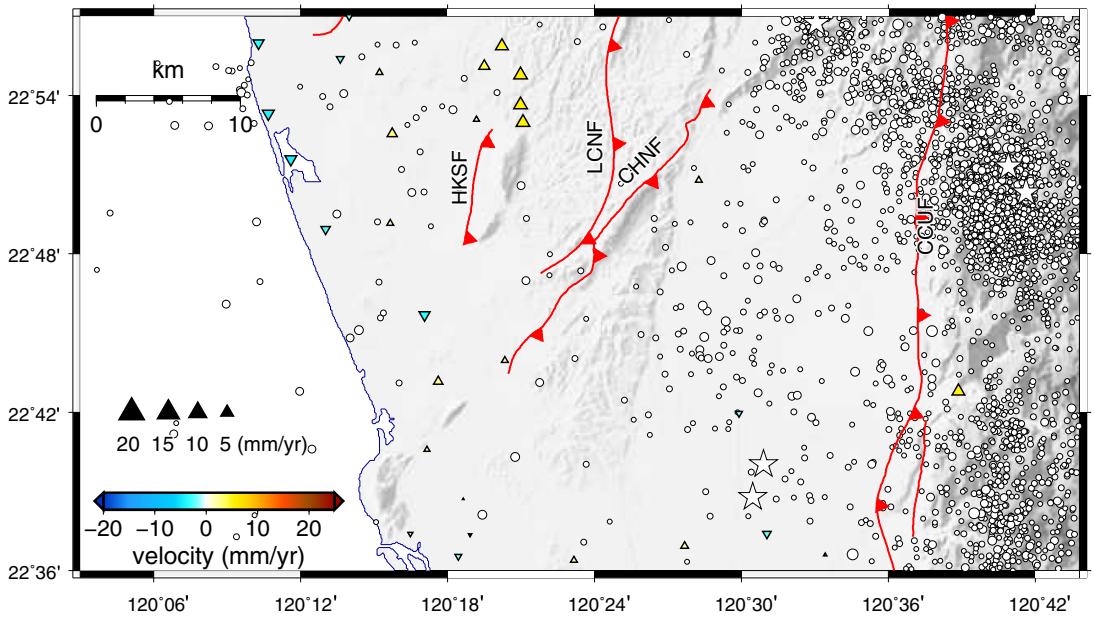

Fig. 7. Longer-term vertical velocity field. These rates which are inferred from the radiometric dates at river terraces or boreholes are collected by Ching et al. (2011a). Warm-colored triangles denote uplift while cool-colored inverse triangles represent subsidence. Color scale shows the magnitude of the vertical velocity. Red lines denote the locations of the active faults. HKSF: the Hsiaokangshan fault, LCNF: the Lungchuan fault, CHNF: the Chishan fault, CCUF: the Chaochou fault. White circles are background seismicity from 1900 to 2010 with $M_L > 2$. Most of their magnitudes are smaller than 3 while white stars denote $M_L > 5$ earthquakes. (For interpretation of the references to color in this figure legend, the reader is referred to the web version of this article.)

8. Conclusions

In this study, 106 campaign-mode GPS observations and 310 Leveling vertical measurements from 2000 to 2010 indicate a significant horizontal velocity gradient of ~15 mm/yr and the maximum uplift rate of ~18 mm/yr located between the HKSF and the CHNF. However, our geodetic data does not fit the 2D dislocation model well. Therefore another mechanism must be considered. In terms of our field investigations, the Gtk has been rising relative to surrounding geologic units, which is interpreted as an onshore mud diapir dominated by vertical tectonics. However the complexity of the arc–continent collision of Taiwan cannot rule out the influence of fold-and-thrust kinematics and southwest lateral extrusion especially as the collision propagates southward through time (Fig. 6). In addition, the HKSF and the CHNF are reverse faults with dextral strike-slip components. The HKSF in the mudstone area is proposed to be a buried creeping fault with low earthquake potential. The CHNF or the décollement here still has the possibility to generate destructive earthquakes in SW Taiwan in the future.

Supplementary data to this article can be found online at http://dx.doi.org/10.1016/j.tecto.2015.07.020.

Acknowledgments

We thank the Central Geological Survey for providing the campaign-mode GPS data. We thank the Central Weather Bureau, Ministry of Interior, Central Geological Survey and Institute of Earth Sciences, Academia Sinica for providing the continuous GPS data. We thank Michael W. Hamburger and Kaj M. Johnson for many helpful suggestions. Figures were generated using the Generic Mapping Tools (GMT), developed by Wessel and Smith (1991). This research was supported by Taiwan NSC grant NSC 102-2116-M-006-017-.

References

Altamimi, Z., Collilieux, X., Legrand, J., Garayt, B., Boucher, C., 2007. ITRF2005: a new release of the International Terrestrial Reference Frame based on time series of station positions and Earth Orientation Parameters. J. Geophys. Res. 112, B09401. http://dx.doi.org/10.1029/2007JB004949.

Angelier, J., Barrier, E., Chu, H.T., 1986. Plate collision and paleostress trajectories in a fold–thrust belt: the Foothills of Taiwan. Tectonophysics 125, 161–178.

Barrier, E., Angelier, J., 1986. Active collision in eastern Taiwan: the coastal Range. Tectonophysics 125, 39–72.

Bos, A.G., Spakman, W., Nyst, M.C.J., 2003. Surface deformation and tectonic setting of Taiwan inferred from a GPS velocity field. J. Geophys. Res. 108, 2458. http://dx.doi.org/10.1029/2002JB002336.

Byrne, T., Chan, Y.-C., Rau, R.-J., Lu, C.-Y., Lee, Y.-H., Wang, Y.-J., 2011. The Arc–Continent Collision in Taiwan. In: Brown, D., Ryan, P.D. (Eds.), Frontiers in Earth Sciences http://dx.doi.org/10.1007/978-3-540-88558-0_8.

Chang, C.P., Chang, T.Y., Angelier, J., Kao, H., Lee, J.C., Yu, S.B., 2003. Strain and stress field in Taiwan oblique convergent system: constraints from GPS observations and tectonic data. Earth Planet. Sci. Lett. 214, 115–127.

Chen, B.C., 2005. A Study on the Southern Part of Chishan Fault (M.S. Thesis), Natl. Cheng Kung Univ, Tainan (125 pp.).

Chen, K.H., Yang, M., Huang, Y.T., Ching, K.E., Rau, R.J., 2011. Vertical displacement rate field of Taiwan from geodetic levelling data 2000–2008. Surv. Rev. 43, 296–302.

Cheng, H.C., 2000. Structural Geology in the Tainan to Pingtung Area of Southwestern Taiwan (M.S. Thesis), Natl. Central Univ, Taoyuan (92 pp.).

Cheng, S.N., Yeh, Y.T., 1989. Catalog of the Earthquakes in Taiwan From 1604 to 1988. Inst. Earth Sci., Academia Sinica IES-R-661, (255 pp.).

Ching, K.E., Rau, R.J., Lee, J.C., Hu, J.C., 2007a. Contemporary deformation of tectonic escape in SW Taiwan from GPS observations, 1995–2005. Earth Planet. Sci. Lett. 262, 601–619.

Ching, K.E., Rau, R.J., Zeng, Y., 2007b. Coseismic source model of the 2003 M_w 6.8 Chengkung earthquake, Taiwan, determined from GPS measurements. J. Geophys. Res. 112, B06422. http://dx.doi.org/10.1029/2006JB004439.

Ching, K.E., Hsieh, M.L., Johnson, K.M., Chen, K.H., Rau, R.J., Yang, M., 2011a. Modern vertical deformation rates and mountain building in Taiwan from precise leveling and continuous GPS observations, 2000–2008. J. Geophys. Res. 116, B08406. http://dx.doi.org/10.1029/2011JB008242.

Ching, K.E., Rau, R.J., Johnson, K.M., Lee, J.C., Hu, J.C., 2011b. Present-day kinematics of active mountain building in Taiwan from GPS observations during 1995–2005. J. Geophys. Res. 116, B09405. http://dx.doi.org/10.1029/2010JB008058.

Chiu, J.-K., Tseng, W.-H., Liu, C.-S., 2006. Distribution of gassy sediments and mud volcanoes offshore southwestern Taiwan. Terr. Atmos. Ocean. Sci. 17, 703–722.

Chou, J.T., 1971. A preliminary study of the stratigraphy and sedimentation of the mudstone formations in the Tainan area, southern Taiwan. Petrol. Geol. Taiwan 8, 187–219.

Chuang, H.-J., 2006. Distribution and Structural Relationships of Mud Diapirs Offshore Southwestern Taiwan (M.S. Thesis), Natl. Taiwan University, Taipei (113 pp.).

Dach, R., Hugentobler, U., Fridez, P., Meindl, M. (Eds.), 2007. Bernese GPS Software Version 5.0. Astronomical Institute, University of Berne (612 pp.).

Donath, F.A., Parker, R.B., 1964. Folds and folding. Bull. Seismol. Soc. Am. 75, 45–62.

Franek, P., Mienert, J., Buenz, S., Géli, L., 2014. Character of seismic motion at a location of a gas hydrate-bearing mud volcano on the SW Barents Sea margin. J. Geophys. Res. 119, 6159–6177. http://dx.doi.org/10.1002/2014JB010990.

Fukuda, J., Johnson, K.M., 2008. A fully Bayesian inversion for spatial distribution of fault slip with objective smoothing. Bull. Seismol. Soc. Am. 98, 1128–1146.

Gourley, J.R., 2006. Syn-tectonic Extension and Lateral Extrusion in Taiwan: The Tectonic Response to a Basement High Promontory (Ph. D. Thesis), Univ. Connecticut, Connecticut (129 pp.).
Gourley, J.R., Lee, Y.-H., Ching, K.-E., 2012. Vertical fault mapping within the Gutingkeng Formation of southern Taiwan: implications for sub-aerial mud diapir tectonics. Abstract T53B-2699 Presented at 2012 Fall Meeting, AGU, San Francisco, Calif., 3–7 Dec.
Harris, R.A., Segall, P., 1987. Detection of a locked zone at depth on the Parkfield, California, segment of the San Andreas Fault. J. Geophys. Res. 92, 7945–7962.
Hedberg, H.D., 1974. Relation of methane generation to undercompacted shales, shale diapirs and mud volcanoes. Am. Assoc. Pet. Geol. Bull. 58, 661–673.
Ho, C.S., 1986. A synthesis of the geologic evolution of Taiwan. Tectonophysics 125, 1–16.
Hsieh, S.H., 1970. Geology and gravity anomalies of the Pingtung Plain, Taiwan. Proc. Geol. Soc. China 13, 76–89.
Hsieh, S.H., 1972. Subsurface geology and gravity anomalies of the Tainan and Chungchou structure of the coastal plain of southwestern Taiwan. Petrol. Geol. Taiwan 10, 323–338.
Hsu, T.L., Chang, H.C., 1979. Quaternary faulting in Taiwan. Mem. Geol. Soc. China 3, 155–165.
Hsu, Y.-J., Simons, M., Yu, S.-B., Kuo, L.-C., Chen, H.-Y., 2003. A two-dimensional dislocation model for interseismic deformation of the Taiwan mountain belt. Earth Planet. Sci. Lett. 211, 287–294.
Hsu, Y.J., Yu, S.B., Simons, M., Kuo, L.C., Chen, H.Y., 2009. Interseismic crustal deformation in the Taiwan plate boundary zone revealed by GPS observations, seismicity, and earthquake focal mechanisms. Tectonophysics 479, 4–18.
Hu, J.C., Hou, C.S., Shen, L.C., Chan, Y.C., Chen, R.F., Huang, C., Rau, R.J., Chen, K.H., Lin, C.W., Huang, M.H., Nien, P.F., 2007. Fault activity and lateral extrusion inferred from velocity field revealed by GPS measurements in the Pingtung area of southwestern Taiwan. J. Asian Earth Sci. 31, 287–302.
Huang, Y.-L., 1995. Distribution of Mud Diapirs Offshore Southwestern Taiwan, Their Relationship to the Onland Anticlinal Structures and Their Effects on the Deposition Environment in Southwest Taiwan (in Chinese) (M.S. Thesis) Natl. Taiwan University, Taipei.
Huang, C.Y., Wu, W.Y., Chang, C.P., Tsao, S., Yuan, P.B., Lin, C.W., Xia, K.Y., 1997. Tectonic evolution of accretionary prism in the arc–continent collision terrane of Taiwan. Tectonophysics 281, 31–51.
Huang, S.T., Yang, K.M., Hung, J.H., Wu, J.C., Ting, H.H., Mei, W.W., Hsu, S.H., Lee, M., 2004. Deformation front development at the northeast margin of the Tainan basin, Tainan–Kaohsiung area, Taiwan. Mar. Geophys. Res. 25, 139–156.
Jenyon, M.K., 1986. Salt Tectonics. Elsevier Applied Science, London (191 pp.).
Johnson, K.M., Segall, P., Yu, S.B., 2005. A viscoelastic earthquake cycle model for Taiwan. J. Geophys. Res. 110, B10404. http://dx.doi.org/10.1029/2004JB003516.
Kopf, A.J., 2002. Significance of mud volcanism. Rev. Geophys. 40 (2), 1005. http://dx.doi.org/10.1029/2000RG000093.
Kostrov, V.V., 1974. Seismic moment and energy of earthquakes and seismic flow of rock. Izv. Acad. Sci. USSR Phys. Solid Earth 1, 13–21 (English Transl.).
Lacombe, O., Angelier, J., Chen, H.W., Deffontaines, B., Chu, H.T., Rocher, M., 1997. Syndepositional tectonics and extension–compression relationships at the front of the Taiwan collision belt: a case study in the Pleistocene reefal limestones near Kaohsiung, SW Taiwan. Tectonophysics 274, 83–96.
Lacombe, O., Mouthereau, F., Deffontaines, B., Angelier, J., Chu, H.T., Lee, C.T., 1999. Geometry and Quaternary kinematics of fold-and-thrust units of southwestern Taiwan. Tectonics 18, 1198–1223.
Lacombe, O., Mouthereau, F., Angelier, J., Deffontaines, B., 2001. Structural, geodetic and seismological evidence for tectonic escape in SW Taiwan. Tectonophysics 333, 323–345.
Lacombe, O., Angelier, J., Mouthereau, F., Chu, H.T., Deffontaines, B., Lee, J.-C., Rocher, M., Chen, R.-F., Siame, L., 2004. The Liuchiu Hsu island offshore SW Taiwan: tectonic versus diapiric anticline development and comparisons with onshore structures. Compt. Rendus Geosci. 336, 815–825.
Lin, A.T., Watts, A.B., 2002. Origin of the West Taiwan Basin by orogenic loading and flexure of a rifted continental margin. J. Geophys. Res. 107, 2185. http://dx.doi.org/10.1029/2001JB000669.
Magara, K., 1978. Compaction and fluid migration. Developments in Petroleum Science 9. Elsevier, New York (320 pp.).
Moreno, M., Rosenau, M., Oncken, O., 2010. 2010 Maule earthquake slip correlates with pre-seismic locking of Andean subduction zone. Nature 467, 198–202.
Mouthereau, F., Deffontaines, B., Lacombe, O., Angelier, J., 2002. Variation along the strike of the Taiwan thrust belt: basement control on structural style, wedge geometry, and kinematics. In: Byrne, T.B., Liu, C.-S. (Eds.), Geology and Geophysics of an Arc–Continent Collision, Taiwan. Geol. Soc. Am. Special Papers 358, pp. 31–54.
Murray, J.R., Segall, P., Cervelli, P., Prescott, W., Svarc, J., 2001. Inversion of GPS data for spatially variable slip-rate on the San Andreas Fault near Parkfield, CA. Geophys. Res. Lett. 28, 359–362.
Okada, Y., 1985. Surface deformation due to shear and tensile faults in a half-space. Bull. Seismol. Soc. Am. 75, 1135–1154.
Pan, Y.S., 1968. Interpretation aid seismic coordination of the Bouguer gravity anomalies obtained in southern Taiwan. Petrol. Geol. Taiwan 6, 197–207.
Ramsay, J.G., 1974. Development of chevron folds. Bull. Seismol. Soc. Am. 85, 1741–1754.
Savage, J.C., Simpson, R.W., 1997. Surface strain accumulation and the seismic moment tensor. Bull. Seismol. Soc. Am. 87, 1345–1353.
Shih, T.T., 1967. A survey of the active mud volcanoes in Taiwan and a study of their types and the character of the mud. Petrol. Geol. Taiwan 6, 259–311.
Sobolewski, S., Gourley, J., 2008. A field investigation of fault rocks within the footwall of the active Chishan Fault, southern Taiwan. Eos Trans. AGU 89 (53) (Fall Meet. Suppl., Abstract T51A-1863).
Sumner, R.H., Westbrook, G.K., 2001. Mud diapirism in front of the Barbados accretionary wedge: the influence of fracture zone and North America–South America plate motions. Mar. Pet. Geol. 18, 591–613.
Sun, S.C., 1964. Photogeologic study of the Tainan–Kaohsiung coastal plain area, Taiwan. Petrol. Geol. Taiwan 3, 39–51.
Sun, S.C., Liu, C.S., 1993. Mud diapirs and submarine channel deposits in offshore Kaohsiung–Hengchun, southwest Taiwan. Petrol. Geol. Taiwan 28, 1–14.
Suppe, J., 1984. Kinematics of arc–continent collision, flipping of subduction and back-arc spreading near Taiwan. Mem. Geol. Soc. China 6, 21–33.
Tanner, P.W.G., 1989. The flexural-slip mechanism. J. Struct. Geol. 11, 635–655.
Teng, L.S., 1987. Stratigraphic records of the late Penglai orogeny of Taiwan. Acta Geol. Taiwan 25, 205–224.
Teng, L.S., 1990. Geotectonic evolution of late Cenozoic arc–continent collision in Taiwan. Tectonophysics 183, 57–76.
Tsai, M.-C., Yu, S.-B., Hsu, Y.-J., Chen, H.-Y., Chen, H.-W., 2012. Interseismic crustal deformation of frontal thrust fault system in the Chiayi–Tainan area, Taiwan. Tectonophysics 554–557, 169–184.
Tsan, S.F., Keng, W.P., 1968. The Neogene rocks and major structural features of southwestern Taiwan. Proc. Geol. Soc. China 11, 45–49.
Wessel, P., Smith, W., 1991. Free software helps map and display data. Eos Trans. AGU 72 (441), 445–446.
Yu, S.B., Chen, H.Y., 1994. Global positioning system measurements of crustal deformation in the Taiwan arc–continent collision zone. Terr. Atmos. Ocean. Sci. 5, 477–498.
Yu, S.B., Chen, H.Y., Kuo, L.C., 1997. Velocity field of GPS stations in the Taiwan area. Tectonophysics 274, 41–59.

Please cite this article as: Ching, K.-E., et al., Rapid deformation rates due to development of diapiric anticline in southwestern Taiwan from geodetic observations, Tectonophysics (2015), http://dx.doi.org/10.1016/j.tecto.2015.07.020